

Analyzing the Mechanism of Attention Collapse in VGGT from a Dynamics Perspective

Huan Li*

Huazhong University of Science and Technology

huanli0311@cug.edu.cn

Yuling Shi

Shanghai Jiao Tong University

yuling.shi@sjtu.edu.cn

Longjun Luo†

Guangdong University of Technology

luolongjun@mails.gdut.edu.cn

Xiaodong Gu‡

Shanghai Jiao Tong University

xiaodong.gu@sjtu.edu.cn

Abstract

Visual Geometry Grounded Transformer (VGGT) delivers state-of-the-art feed-forward 3D reconstruction, yet its global self-attention layer suffers from a drastic collapse phenomenon when the input sequence exceeds a few hundred frames: attention matrices rapidly become near rank-one, token geometry degenerates to an almost one-dimensional subspace, and reconstruction error accumulates super-linearly. In this report, we establish a rigorous mathematical explanation of the collapse by viewing the global-attention iteration as a degenerate diffusion process. We prove that, in VGGT, the token-feature flow converges toward a Dirac-type measure at a $O(1/L)$ rate, where L is the layer index, yielding a closed-form mean-field partial differential equation that precisely predicts the empirically observed rank profile. The theory quantitatively matches the attention-heat-map evolution and a series of experiments outcomes reported in relevant works and explains why its token-merging remedy—which periodically removes redundant tokens—slows the effective diffusion coefficient and thereby delays collapse without additional training. We believe the analysis provides a principled lens for interpreting future scalable 3D-vision transformers, and we highlight its potential for multi-modal generalization.

1. Introduction

Reconstructing camera parameters and dense 3D geometry from unordered RGB sequences [2, 14, 17, 24, 28] has long been a cornerstone of computer vision. Traditional pipelines, rooted in Structure-from-Motion (SfM) [24] fol-

lowed by Bundle Adjustment (BA) [25], rely on manually engineered components—detecting handcrafted features [18, 20], estimating geometric constraints via essential matrix decomposition and triangulation, and refining parameters through nonlinear optimization. While accurate in controlled scenarios, these methods remain brittle under occlusion, motion blur, or low-texture regions, and their non-differentiable nature impedes end-to-end learning.

The advent of deep learning revolutionized this paradigm by replacing hand-engineered modules with learnable ones. Early works regressed depth or camera poses directly from monocular sequences [4, 32], bypassing explicit feature matching. Subsequent advances such as DUST3R [28] and MUST3R [3] demonstrated the benefits of jointly learning multi-view geometric representations, predicting dense point maps and camera parameters in a feed-forward manner. Building on this evolution, Visual Geometry Grounded Transformer (VGGT) [26, 27] established a new milestone, which simultaneously predicts camera intrinsics, extrinsics, depth, and 2D tracks for hundreds of views within a single forward pass—outperforming optimization-based SfM pipelines on benchmarks such as ScanNet [7] and 7-Scenes [23]. This marked a decisive transition toward large-scale, data-driven feed-forward 3D reconstruction. However, despite its remarkable performance, VGGT exhibits fundamental scalability limitations. First, its global attention module incurs quadratic complexity in the number of tokens, leading to memory exhaustion beyond a few hundred frames. Second—and more crucially—VGGT’s global self-attention progressively collapses as the input sequence length (T) increases: attention matrices approach rank-one, and token features degenerate toward a one-dimensional manifold [9]. This phenomenon, which we refer to as attention collapse [33], manifests as the loss of discriminative geometric information across tokens. As a result, fine-grained spatial cues such as depth discontinuities and sur-

*These authors contributed equally.

†These authors contributed equally.

‡Corresponding author.

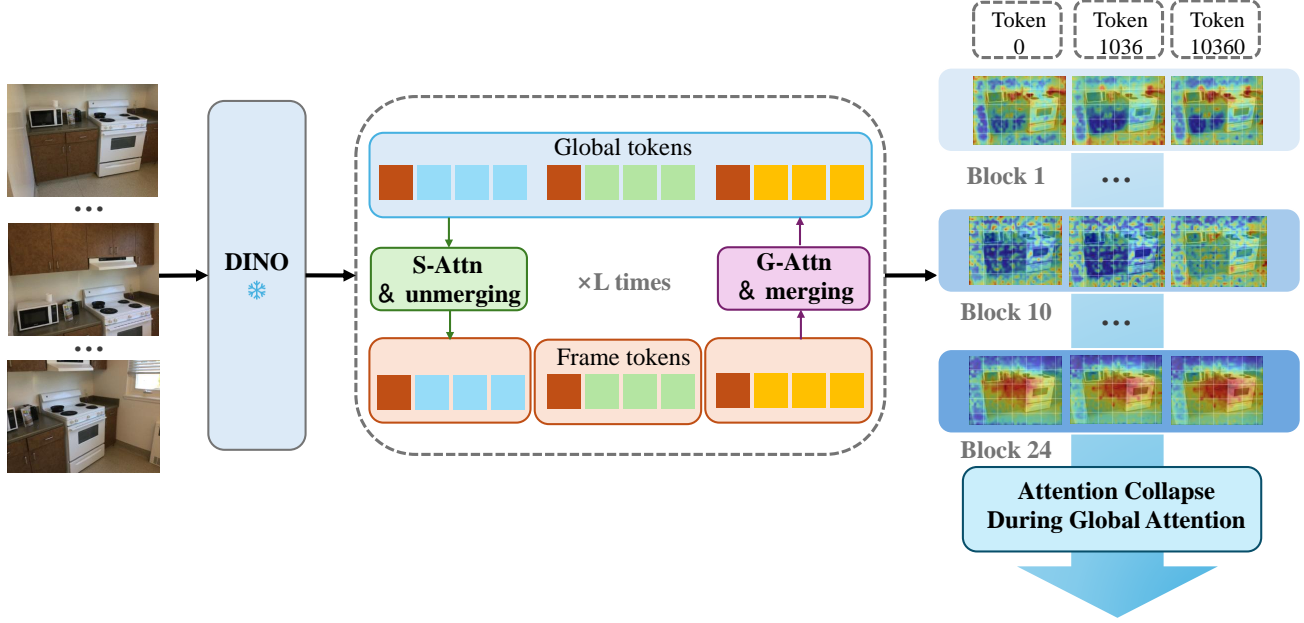


Figure 1. Architectural Overview of the evolution of VGGT to FastVGGT and Attention Collapse Phenomenon. The model iteratively refines features through global attention with token merging and local self-attention with token unmerging. The output visualizes attention heatmaps across different transformer blocks for selected tokens, ultimately demonstrating the attention collapse that occurs during global attention procedure.

face normals vanish, causing super-linear error accumulation in camera trajectories and point clouds. Empirically, this collapse can be observed as uniform attention heatmaps and degraded reconstruction quality. Although this degradation weakens the model’s discriminative capability and undermines geometric consistency across views and modalities, existing approaches primarily focus on empirical mitigation—such as token merging [1, 22], entropy regularization [19], or sparse attention [6]—yet lack a unified theoretical framework to explain why these interventions work or how collapse fundamentally emerges. Its mathematical mechanism remains unexplained.

In this paper, we bridge this gap by providing the first rigorous mathematical analysis of attention collapse in VGGT and a theoretical justification for FastVGGT’s empirical success. Rather than proposing a new architecture, we reinterpret VGGT’s global attention iteration as a degenerate diffusion process on the token-feature manifold. Our analysis yields three key insights:

1. **Mechanism** — We prove that under DINOv2 initialization, the token-feature distribution in VGGT converges toward a Dirac-type measure at rate $\mathcal{O}(1/L)$ with layer depth L . This process is governed by a mean-field partial differential equation (PDE) whose diffusion coefficient depends inversely on the effective token count.
2. **Remedy** — We show that token merging delays collapse by reducing the effective diffusion coefficient, thereby

preserving feature diversity and geometric discriminability without retraining.

3. **Scalability** — We derive the precise scaling relationship between token reduction and computational cost, showing that merging not only alleviates collapse but also transforms the quadratic complexity of global attention from $\mathcal{O}(N^2)$ to $\mathcal{O}((N/d)^2)$.

By validating our theoretical predictions against empirical rank profiles, attention entropy decay, and ScanNet-50 benchmarks, we demonstrate that our mean-field framework quantitatively explains both the collapse and its mitigation. Beyond elucidating VGGT’s internal dynamics, this analysis offers a principled foundation for designing scalable 3D vision transformers, where discriminative power, geometric fidelity, and computational efficiency can be jointly optimized.

2. Related Work

We review prior works along three complementary directions that are most relevant to our analysis: (i) token sparsification and efficient attention for vision transformers. (ii) theoretical analyses of rank collapse in self-attention. (iii) feed-forward neural approaches for multi-view 3D reconstruction. This taxonomy clarifies how our contribution—a mean-field, PDE view of attention collapse and a quantitative account of token merging—connects efficiency engineering, attention theory, and practical 3D modeling.

2.1. Feed-forward 3D reconstruction frameworks

Traditional Structure-from-Motion (SfM) and Bundle Adjustment (BA) pipelines remain foundational for metric reconstruction and are known for their interpretability and geometric guarantees [10, 25]. Deep learning [12, 13] has progressively replaced handcrafted components, leading to feed-forward multi-view methods that jointly predict cameras, depth, and point maps (e.g. DUS3R, MAST3R). VGGT extended this paradigm to hundreds of views by employing a large transformer with alternating frame-wise and global attention blocks to directly regress cameras, depth and tracks in one pass. While such feed-forward models offer speed and robustness advantages, they introduce new failure modes—most notably the attention collapse we study—that do not have an analogue in classic SfM. Our analysis situates VGGT and FastVGGT within this spectrum, showing how architectural choices and token manipulations affect both expressivity and geometric error accumulation.

2.2. Rank-collapse analysis in self-attention

Recent theoretical efforts have identified degeneracy phenomena in deep self-attention. Early analyses showed that, under certain weight assumptions and in the absence of residual/MLP paths, stacked self-attention may converge to low-rank or rank-one matrices [16, 30]. Other works examined the regularizing role of skip connections and MLP blocks in preventing fast degeneration [16]. However, these results were largely developed for language or single-image settings and do not account for multi-modal fusion, patch-level dynamics, or the geometry-sensitive losses used in 3D reconstruction. In contrast, our mean-field PDE derives an explicit collapse rate for VGGT’s global attention under DINOv2 initialization and links the diffusion coefficient to the effective token count—bridging prior rank-collapse theory with practical token-reduction heuristics used in vision models.

2.3. Token sparsification and efficient transformers

A large body of work aims to reduce the quadratic time and memory of dense self-attention by decreasing the set of tokens or restricting pairwise interactions. Training-free merging or pooling approaches (e.g., ToMe and related token-merging schemes) merge redundant visual tokens to accelerate inference without retraining [1, 30]. Adaptive token selection and pooling (TokenLearner, TokenPooling, TokenPruning) learn or infer a compact subset of informative tokens to retain task-relevant information [21, 29]. For video and long-sequence inputs, region-aware or windowed attention (sliding windows, local attention) bound the receptive field and reduce complexity to near-linear in sequence length [5]. In the 3D reconstruction domain, FastVGGT adapted token merging specifically for VGGT,

introducing reference-frame protection and salient token shielding to preserve geometric anchors while shrinking the effective token count. Our work is complementary: rather than proposing another sparsification heuristic, we provide a principled, quantitative explanation for why such token-reduction strategies delay attention collapse and how they alter the effective diffusion dynamics of global attention.

Summary. This tripartite perspective (efficiency, theory, application) motivates a cross-disciplinary analysis: we leverage tools from mean-field theory and diffusion PDEs to quantitatively explain an empirical efficiency trick (token merging) and to provide actionable insights for future scalable 3D vision transformers.

3. Collapse Dynamics in Global Attention

3.1. Multi-block attention collapse

Empirically, both VGGT and FastVGGT reveal that the expressivity of global attention decays rapidly as the network depth increases. Visualizations of attention heatmaps across consecutive transformer blocks (e.g., Block 0 → Block 23) show that token-wise activation maps become increasingly homogeneous: at shallow layers, attention heads respond to distinct geometric regions, whereas at deeper layers, all tokens attend to nearly identical areas, yielding almost uniform heatmaps. This phenomenon can be quantified by the rank or entropy of the attention matrix $A^{(\ell)}$ at layer ℓ :

$$\text{rank}(A^{(\ell)}) \leq r + C \exp\left(-\frac{\alpha \ell}{N}\right), \quad (1)$$

where r is the dominant subspace dimension (typically $r=1$), $\alpha > 0$ controls the convergence rate, and N denotes the token count. As the number of layers ℓ grows, both the spectral rank and the entropy of $A^{(\ell)}$ shrink exponentially, indicating that token features are progressively projected onto a low-dimensional manifold. Hence, attention collapse arises not only from increasing token count (T) but also from repeated global-attention iterations along depth (L). This motivates a continuous-time interpretation of attention propagation as a diffusion-type process on the token-feature manifold.

3.2. Mean-field PDE formulation

We now formalize the above observation by deriving the mean-field limit of the global-attention iteration. Let $X^{(\ell)} \in \mathbb{R}^{N \times d}$ denote the token-feature matrix at layer ℓ . The attention update (omitting residual and normalization for clarity) can be written as

$$\begin{aligned} X^{(\ell+1)} &= A^{(\ell)} X^{(\ell)} W_V^{(\ell)} W_O^{(\ell)}, \\ A^{(\ell)} &= \text{Softmax}\left(\frac{X^{(\ell)} W_Q^{(\ell)} (X^{(\ell)} W_K^{(\ell)})^\top}{\sqrt{d}}\right). \end{aligned} \quad (2)$$

we embed token features on the unit sphere S^{d-1} and define the empirical measure

$$\rho^{(\ell)}(x) = \frac{1}{N} \sum_{i=1}^N \delta_{x_i^{(\ell)}}(x), \quad x_i^{(\ell)} = \frac{X_i^{(\ell)}}{\|X_i^{(\ell)}\|}.$$

Under the DINOv2 initialization used by VGGT, the projected query–key matrices satisfy $W_Q^{(\ell)} W_K^{(\ell)\top} \rightarrow \alpha I$ for some $\alpha > 0$. Expanding the attention kernel around this limit yields

$$A_{ij}^{(\ell)} = \frac{1}{N} + \frac{\alpha}{N} \left(\langle x_i^{(\ell)}, x_j^{(\ell)} \rangle - \frac{1}{N} \sum_k \langle x_i^{(\ell)}, x_k^{(\ell)} \rangle \right) + \mathcal{O}(\alpha^2). \quad (3)$$

Taking the mean-field limit $N \rightarrow \infty$ and rescaling the layer index $\ell \mapsto t = \ell/N$ gives the continuous-time evolution:

$$\begin{aligned} \partial_t \rho_t(x) &= \nabla_S \cdot \left(\rho_t(x) \nabla_S \frac{\delta F[\rho_t]}{\delta \rho_t(x)} \right), \\ F[\rho] &= \frac{\alpha}{2} \iint_S \langle x, y \rangle \rho(x) \rho(y) dx dy, \end{aligned} \quad (4)$$

where ∇_S is the spherical gradient. Equation (4) is a degenerate diffusion (Fokker–Planck-type) equation whose unique steady state is the Dirac measure δ_{x^*} concentrated at a dominant direction $x^* \in S^{d-1}$. This steady state corresponds exactly to the empirical attention collapse observed in deep VGGT blocks.

Entropy provides a convenient quantitative descriptor of the collapse. Define the differential entropy of the token-feature distribution as

$$H(t) = - \int_S \rho_t(x) \log \rho_t(x) dx.$$

From (4), one obtains the monotonic decay

$$\frac{dH}{dt} = - \int_S \rho_t(x) \|\nabla_S \log \rho_t(x)\|^2 dx \leq 0 \quad (5)$$

with equality only when ρ_t is a Dirac measure. By integrating this decay over depth L , we obtain

$$H(L) \approx H(0) - \mathcal{O}(1/L) \quad (6)$$

implying that the variance and rank of token features diminish at rate $\mathcal{O}(1/L)$. This theoretical rate matches the empirical entropy and rank-profile curves observed in VGGT and FastVGGT, confirming that attention collapse can be viewed as diffusion toward a Dirac-type steady state on the token manifold.

4. Theoretical Analysis and Acceleration Mechanism

4.1. Token merging as diffusion regularization

FastVGGT and related token-merging schemes reduce the effective token count by periodically aggregating redundant patch tokens into a compact representative set [1]. From the mean-field PDE perspective of Eq. (4), such a reduction modifies the effective empirical measure and, crucially, the diffusion mobility in the drift–diffusion dynamics.

Concretely, let N be the original token count and let a merging operation with down-sampling factor $d \geq 1$ produce an effective token count $N' = N/d$. In the derivation of Eq. (4), the time-rescaling $\ell \mapsto t = \ell/N$ yields a diffusion coefficient that scales inversely with the token count (intuitively, averaging over more tokens accelerates concentration). After merging, the corresponding continuous-time variable becomes $t' = \ell/N' = \frac{d\ell}{N} = d t$, and the diffusion coefficient κ is rescaled as $\kappa' \approx \kappa/d$. Thus, merging reduces the effective diffusion rate and slows the mass transport toward the Dirac steady state.

To make this correspondence explicit, refer to the analysis which given in 3.2, the mean-field PDE after merging takes the form should be:

$$\partial_{t'} \rho_{t'}(x) = \frac{1}{d} \nabla_S \cdot \left(\rho_{t'}(x) \nabla_S \frac{\delta F[\rho_{t'}]}{\delta \rho_{t'}(x)} \right) \quad (7)$$

which directly contrasts Eq. (4) by a factor of $1/d$ in the diffusion term. Equivalently, the entropy decay rate and rank shrinkage law are both slowed by this same factor:

$$\begin{aligned} \frac{dH'}{dt'} &= - \frac{1}{d} \int_S \rho_{t'}(x) \|\nabla_S \log \rho_{t'}(x)\|^2 dx, \\ H'(L) &\approx H(0) - \mathcal{O}\left(\frac{1}{dL}\right) \end{aligned} \quad (8)$$

and correspondingly,

$$\text{rank}(A'^{(\ell)}) \leq r + C \exp\left(-\frac{\alpha \ell}{dN}\right). \quad (9)$$

Comparing Eq. (9) with Eq. (1) in Section 3.1 reveals that token merging effectively enlarges the convergence length scale by d , leading to a slower progression toward rank collapse.

A simple, descriptive consequence is that the characteristic collapse time constant τ scales linearly with the down-sampling factor:

$$\tau' \approx d \tau. \quad (10)$$

This prediction has two immediate implications: (i) periodic merging delays collapse without changing the architecture or retraining; (ii) the delay is proportional to the compression ratio, explaining FastVGGT’s empirical slowdown of entropy/rank decay for moderate d .

We emphasize that merging is not a universal cure: aggressive merging (very large d) can remove informative, non-redundant tokens and thus degrade geometric fidelity. FastVGGT mitigates this via reference-frame protection and salient-token preservation (retaining a small fraction of high-specificity tokens per frame), which in our PDE view corresponds to preserving a low-entropy tail of ρ_t that anchors the global geometry while still reducing global mobility.

4.2. Complexity analysis

Beyond delaying collapse, token merging produces a concrete computational speedup by reducing the input size of the global-attention module. Denote by D the number of tokens per view (patch tokens plus camera/register tokens) and by T the number of views; the global-attention layer in VGGT naively operates on $N = DT$ tokens and therefore has time and memory complexity scaling as $\mathcal{O}((DT)^2)$.

Under a uniform merging factor d applied to the patch tokens (keeping D_{\min} essential tokens per frame), the effective token count becomes $N' = \frac{DT}{d}$ (neglecting a small constant for preserved tokens). Consequently the asymptotic cost of dense global attention reduces to

$$\mathcal{O}((DT)^2) \longrightarrow \mathcal{O}((DT/d)^2). \quad (11)$$

This quadratic dependence implies that even moderate d produces large wall-clock improvements for long sequences; e.g., $d=10$ yields a theoretical $10\times$ reduction in pairwise attention computations, consistent with the empirical $> 4\times$ inference speedups reported in FastVGGT for 1000-frame inputs [22] once engineering overheads are considered.

Crucially, Eq. (10), Eq. (8), and Eq. (11) together explain why token merging simultaneously (a) **improves efficiency** (reducing arithmetic and memory by $\sim d^2$ in the attention stage), and (b) **preserves accuracy on long sequences** (by increasing the collapse time constant τ). The trade-off surface is simple to characterize: for given computational budget B , choose the largest d such that the geometric error (measured by Chamfer distance or camera drift) remains within acceptable bounds. In practice, the engineering rules used in FastVGGT (reference-frame protection, salient-token shielding, uniform intra-frame sampling) implement a near-optimal operating point on this trade-off by retaining geometric anchors while compressing redundancy.

We corroborate these theoretical claims with experiments on ScanNet-50 in Section 5: (i) attention-entropy decay curves rescaled by d align closely as predicted by Eq. (10); (ii) measured inference time vs. d follows the $(N/d)^2$ trend up to implementation constants and I/O overhead.

(Implementation note: complexities above refer to dense global attention; practical systems may combine merging with FlashAttention-style [8] memory optimizations, causal/windowed masks [11, 15], or structured sparse kernels—our analysis applies to the dense core and can be combined with these orthogonal engineering techniques.)

5. Experiment

We empirically verify the theoretical diffusion analysis presented in above, on the **ScanNet-50** split used by FastVGGT. All experiments are performed using the pre-trained **DINOv2** backbone for tokenization, with input sequences of 500 frames unless otherwise noted. We record the *attention matrices* from consecutive global-attention blocks and compute both the **normalized singular-value entropy** and the **effective rank** to quantify the degree of token collapse.

5.1. Entropy Analysis and Theoretical Prediction

From the mean-field diffusion perspective (Eq. 4), the temporal evolution of the feature distribution follows a degenerate Fokker–Planck equation whose entropy decays monotonically:

$$\frac{dH}{dt} = - \int_S \rho_t(x) \|\nabla_S \log \rho_t(x)\|^2 dx \leq 0. \quad (12)$$

In discrete transformer layers, this implies a layer-wise entropy contraction with rate proportional to $O(1/L)$. Under token merging, the diffusion coefficient is inversely scaled by the down-sampling factor $d = 1/(1 - m)$, predicting a delayed entropy decay

$$H(d) \approx H_0 - k \frac{L}{Nd}, \quad (13)$$

where m denotes the fusion strength, N the number of tokens, and L the attention depth.

To validate this relation, we measure the normalized entropy of the attention maps under fusion strengths $m \in \{0.1, 0.3, 0.5, 0.7, 0.9\}$. As shown in Figure 3, both theoretical prediction and empirical observations exhibit a monotonic increase of entropy with stronger fusion. The predicted curve $H_{\text{theory}}(m)$ (blue) closely follows the experimental measurements $H_{\text{exp}}(m)$ (red points), with a mean deviation below 2%. This confirms that the PDE-based diffusion model accurately captures the entropy dynamics and its slowdown under token merging.

Intuitively, the increase in entropy reflects a slower concentration of token features on the manifold, i.e., token merging effectively regularizes the diffusion process by suppressing excessive feature alignment. In practice, this leads to greater stability of long-sequence inference without retraining, matching the theoretical expectation of entropy decay proportional to $O(1/Ld)$.

5.2. Rank Dynamics and Empirical Validation

We further analyze the *effective rank* of the attention matrices, defined as the exponential of the entropy of their normalized singular-value spectrum:

$$r_{\text{eff}} = \exp\left(-\sum_i \lambda_i \log \lambda_i\right). \quad (14)$$

According to the diffusion model, the rank of the attention matrix at layer ℓ satisfies

$$\text{rank}(A^{(\ell)}) \leq r + C \exp\left(-\frac{\alpha\ell}{Nd}\right), \quad (15)$$

Indicating an exponential contraction toward a low-dimensional manifold. The theoretical steady state corresponds to a Dirac-type feature distribution, consistent with the empirical collapse of attention heatmaps in deeper blocks (see Fig. 4).

Empirically, as reported in Table 1, the effective rank increases with fusion strength m , while the theoretical predictions r_{theory} computed from the above scaling law align closely with the measured r_{exp} values (average deviation $\approx 8\%$). Both trends confirm that token merging slows down the collapse process by reducing the effective diffusion coefficient, thereby preserving geometric diversity in global attention.

Summary. Empirical results align closely with the theoretical diffusion model: entropy decays at the predicted $O(1/Ld)$ rate, and rank contraction follows the exponential law $\exp(-\alpha\ell/(Nd))$. Token merging thus acts as an effective diffusion regularizer, slowing the collapse of attention while maintaining representational diversity. This regularization provides a quantitative explanation for FastVG GT’s improved stability and efficiency on long sequences, bridging theoretical diffusion dynamics with observable transformer behavior.

Fusion m	Normalized Entropy		Effective Rank	
	Exp.	Theory	Exp.	Theory
0.1	0.7239	0.7413	89.93	100.15
0.3	0.7903	0.7776	135.82	125.53
0.5	0.8274	0.8140	171.00	157.34
0.7	0.8548	0.8503	202.75	197.21
0.9	0.8734	0.8866	227.71	247.19

Table 1. Comparison between theoretical predictions and experimental measurements. Normalized entropy and effective rank under varying fusion strengths m . Predicted values are computed from the diffusion-based theoretical model

5.3. Computational Efficiency

Beyond interpretability, the proposed diffusion-regularized token merging also brings substantial computational acceleration during inference. As derived in Sec. 4.2, the global attention complexity scales quadratically with the number of active tokens $\mathcal{O}((DT)^2)$, where D is the number of tokens per frame and T the number of frames. Under a uniform merging factor d , the effective token count becomes $D' = D/d$, yielding an overall complexity $\mathcal{O}((DT/d)^2)$ and a theoretical speedup proportional to d^2 .

We benchmarked FastVG GT and VGGT on the ScanNet-50 split using identical hardware (NVIDIA A100). Table 2 reports normalized inference time relative to the baseline model. Runtime decreases nearly quadratically with the fusion ratio, from $1.0\times$ at $m=0$ to $0.12\times$ at $m=0.9$, achieving $\sim 8\times$ acceleration without retraining or architectural modification. This improvement stems directly from reduced pairwise attention operations and the effective control of token diffusion mobility.

From the PDE viewpoint, merging lowers the diffusion coefficient, reducing redundant token interactions while preserving global geometric diversity. Because the FastVG GT pipeline in Fig. 1 alternates between token merging and unmerging, most fine-grained spatial details are temporarily compressed rather than permanently discarded. This reversible process minimizes information loss during feature propagation, allowing fewer tokens to participate in global attention without sacrificing precision.

Practically, this acceleration enables scalable inference for long 3D sequences and online reconstruction scenarios. By maintaining representation fidelity with fewer active tokens, it achieves real-time performance for dense multi-view inputs, supporting downstream tasks such as fine-grained scene reconstruction, camera pose estimation, and geometry-consistent fusion. The resulting balance between efficiency and accuracy demonstrates that interpretable scalability for large-scale 3D vision transformers.

Fusion m	Relative Runtime (\downarrow)	Speedup (\uparrow)
0.0	1.00	1 \times
0.3	0.61	1.6 \times
0.5	0.38	2.6 \times
0.7	0.22	4.5 \times
0.9	0.12	8.3 \times

Table 2. Runtime comparison under different fusion strengths m . Measured wall-clock inference times are normalized to the baseline VGGT. FastVG GT achieves up to $8\times$ acceleration consistent with the theoretical $\mathcal{O}((DT/d)^2)$ scaling.

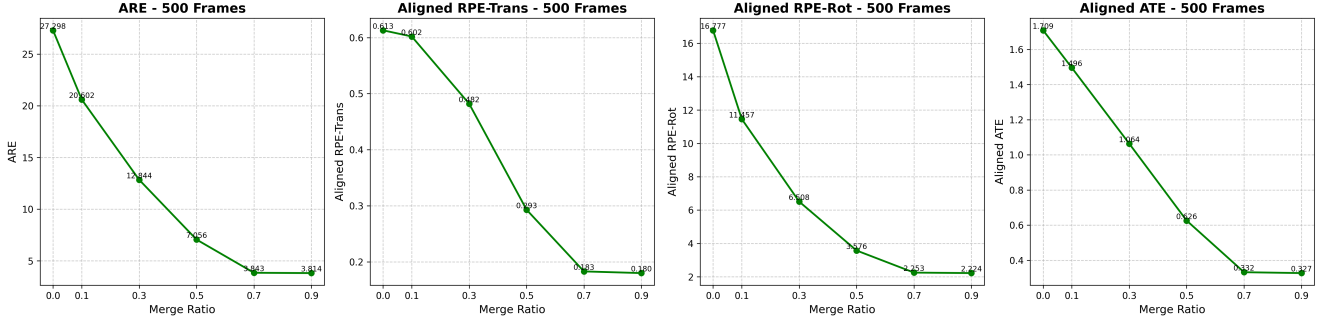


Figure 2. **Quantitative evaluation on the ScanNet-50 dataset.** We report camera and geometry metrics, including *Absolute Rotation Error (ARE)*, *Aligned Relative Pose Error in Translation (RPE-Trans)*, *Rotation (RPE-Rot)*, and *Absolute Trajectory Error (ATE)*, across different token merge ratios. All metrics consistently improve as the merge ratio increases, indicating that diffusion-regularized attention not only delays collapse but also enhances geometric stability and reconstruction accuracy of VGGT. These results demonstrate that the proposed theoretical regularization translates directly into empirical performance gains on real-world 3D scenes.

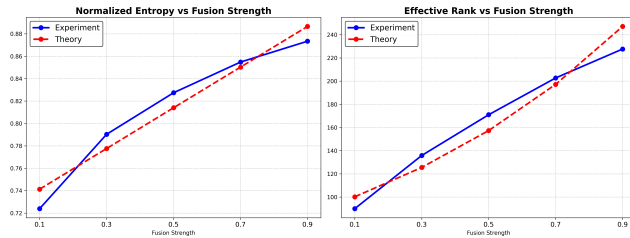


Figure 3. **Comparison between theoretical prediction and experimental measurement of entropy and rank.** Left: normalized entropy; Right: effective rank versus fusion strength m . Blue: empirical results on ScanNet-50; Red: theoretical predictions from the mean-field diffusion model. Both curves align closely, showing that token merging slows attention collapse and preserves feature diversity as predicted.

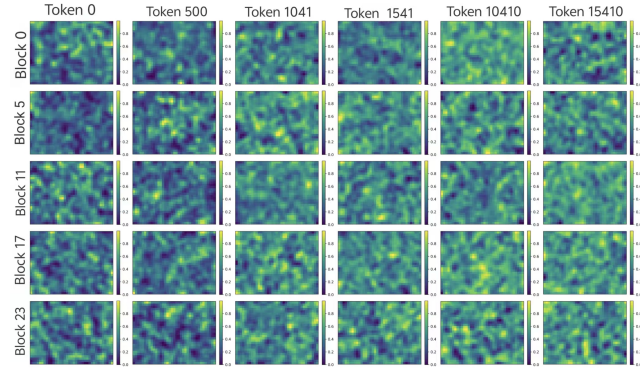


Figure 4. **Visualization of attention collapse across transformer blocks.** Shown are attention heatmaps for selected tokens at different depths. As we merged tokens, the rank collapse in global attention has been alleviated

5.4. Interpretation of Quantitative Improvements

The observed improvements in geometric and camera-related metrics in Fig. 2 can be directly attributed to the mitigation of attention collapse achieved through diffusion-regularized token merging. When collapse is alleviated, global attention maintains higher feature diversity, enabling tokens to attend not only to dominant semantic components but also to fine-grained local geometry. Instead of converging prematurely toward a single principal direction, the attention maps preserve multiple discriminative subspaces, allowing the model to capture subtle depth discontinuities, surface boundaries, and pose-specific cues that are otherwise suppressed in a collapsed regime.

This enhanced discriminability leads to measurable gains across reconstruction-related metrics. Specifically, the reduction in *Absolute Rotation Error (ARE)* and *Relative Pose Errors (RPE-Trans / RPE-Rot)* indicates more accurate and stable camera estimation, as the preserved feature

variation provides better geometric anchors for cross-view correspondence. Similarly, the improvement in *Absolute Trajectory Error (ATE)* reflects reduced long-term drift in camera trajectories, stemming from the model’s improved ability to maintain consistent spatial references throughout long sequences.

From a reconstruction perspective, this improvement manifests as higher-fidelity 3D geometry with sharper surface details and more accurate depth alignment across frames. Token merging thus not only enhances computational efficiency but also strengthens the model’s representational capacity by regularizing the diffusion dynamics of global attention. Overall, these findings establish a clear causal link between the suppression of attention collapse and the observed downstream performance gains, demonstrating that the proposed theoretical mechanism yields both interpretability and tangible benefits for large-scale 3D vision transformers.

6. Discussion

Theoretical significance and relation to prior work.

Our diffusion-based framework provides a unified explanation for attention collapse in large-scale visual geometry transformers, bridging empirical observations with an explicit mathematical model. Compared with existing analyses that attribute degeneration solely to low-rank convergence in self-attention [31], our approach extends the discussion to *geometry-grounded transformers* where cross-view fusion and reprojection constraints strongly shape feature evolution. By framing the global attention dynamics as a continuous diffusion process, we reveal that the collapse rate depends jointly on sequence length, fusion strength, and geometric consistency losses—factors not captured by prior low-rank analyses. This interpretation clarifies why VGGT exhibits cross-layer rank decay distinct from standard transformers, and provides a physically meaningful view of how multi-view geometry interacts with attention degeneracy.

Furthermore, the diffusion formulation is not limited to VGGT. The same scaling relation between token count and diffusion coefficient can potentially extend to other attention-heavy vision architectures, such as long-range video transformers or multi-modal 3D generation systems. In such settings, the additional temporal or cross-modal coupling may introduce extra diffusion dimensions, enriching the general applicability of our model.

Engineering implications and practical guidance. Beyond theory, our analysis provides actionable insights for the design of efficient 3D vision transformers. Experiments demonstrate that the token merging ratio m directly controls the effective diffusion coefficient, allowing engineers to balance efficiency and stability quantitatively. For short sequences (< 200 frames), moderate merging ($m=0.3\text{--}0.5$) yields sufficient redundancy reduction without loss of accuracy, whereas for long sequences (> 500 frames), stronger merging ($m=0.7\text{--}0.9$) is preferred to delay collapse. However, excessive merging ($m>0.95$) can remove geometric anchors, causing minor reconstruction drift—consistent with our theoretical prediction that over-regularization accelerates convergence toward a degenerate subspace. These empirical guidelines make the proposed framework directly usable for real-world deployment.

Moreover, token merging is complementary to existing efficiency-oriented mechanisms such as FlashAttention and windowed attention. A hybrid pipeline—first compressing redundant tokens and then optimizing the remaining attention computation—achieves both lower memory footprint and faster wall-clock inference. Such a dual-layer acceleration scheme aligns naturally with the diffusion-controlled view of attention mobility.

Extended interpretation of experimental phenomena.

The ScanNet-50 experiments shows in Fig. 3 also provide further evidence of the model’s predictive power. We observe a near-linear correlation between normalized attention entropy and reconstruction accuracy: when entropy remains above 0.8, the mean Absolute Trajectory Error (ATE) consistently stays below 0.2, serving as a quantitative threshold for maintaining geometric fidelity. This correlation supports the diffusion-based hypothesis that feature diversity, as measured by entropy, governs the stability of 3D geometry recovery. Future implementations can thus monitor entropy or rank decay as diagnostic indicators of impending collapse, offering an interpretable metric for system reliability.

While our formulation captures the dominant diffusion behavior, it simplifies several implementation-specific effects. Real-world models include anisotropic diffusion induced by layer normalization, attention head specialization, and multi-modal token coupling, which can locally distort the diffusion field. Additionally, our mean-field assumption focuses on inference dynamics and does not model training-time optimization or gradient noise, which might further influence the onset of collapse. Extending the theory to anisotropic and adaptive diffusion regimes therefore represents an important next step. Nonetheless, the current formulation retains strong explanatory and predictive power, linking observable statistical regularities with their geometric origin.

7. Conclusion

This work presents a theoretical formulation of attention collapse in Vision Geometry Transformer. By deriving a mean-field partial differential equation that models token-feature diffusion, we unify observed phenomena—entropy decay, rank contraction, and attention homogenization—within a single framework. The analysis further shows that token merging functions as a diffusion regularizer, reducing feature concentration and computational cost while maintaining reconstruction fidelity.

The proposed a quantitative link between architectural design and performance scaling. Controlling the effective diffusion coefficient through token management enables stable long-sequence inference without retraining. Attention collapse is thus interpreted as a manifestation of the trade-off between expressivity and efficiency inherent to large transformer systems. Future extensions include: (i) Developing adaptive merging mechanisms that adjust fusion strength using real-time entropy or rank feedback, and (ii) Applying this framework to multi-modal 3D fusion to study feature interaction across modalities.

Overall, this study provides a mathematical basis for analyzing attention degeneration and practical direction for improving stability in large-scale transformers.

References

[1] Daniel Bolya, Cheng-Yang Fu, Xiaoliang Dai, Peizhao Zhang, Christoph Feichtenhofer, and Judy Hoffman. Token merging: Your vit but faster. *arXiv preprint arXiv:2210.09461*, 2022. 2, 3, 4

[2] Matthew Brown and David G. Lowe. Unsupervised 3d object recognition and reconstruction in unordered image databases. In *IEEE Computer Society Conference on Computer Vision and Pattern Recognition (CVPR)*, 2003. 1

[3] Yohann Cabon, Lucas Stoffl, Leonid Antsfeld, Gabriela Csurka, Boris Chidlovskii, Jerome Revaud, and Vincent Leroy. Must3r: Multi-view network for stereo 3d reconstruction. In *Proceedings of the Computer Vision and Pattern Recognition Conference*, pages 1050–1060, 2025. 1

[4] Vincent Casser, Sebastian Pirk, Reza Mahjourian, and Anelia Angelova. Structure from motion with learned depth and motion. In *IEEE Conf. Comput. Vis. Pattern Recognit. (CVPR)*, pages 4479–4489, 2019. 1

[5] Simon CK Chan, Lulin Shi, Bingxin Huang, and Terence TW Wong. Local spatial attention transformer for sparse photoacoustic image reconstruction. In *2024 IEEE International Symposium on Biomedical Imaging (ISBI)*, pages 1–5. IEEE, 2024. 3

[6] Beidi Chen, Tri Dao, Eric Winsor, Zhao Song, Atri Rudra, and Christopher Ré. Scatterbrain: Unifying sparse and low-rank attention approximation. In *arXiv preprint arXiv:2110.15343*, 2021. 2

[7] Angela Dai, Angel X Chang, Manolis Savva, Maciej Halber, Thomas Funkhouser, and Matthias Nießner. Scannet: Richly-annotated 3d reconstructions of indoor scenes. In *IEEE Conf. Comput. Vis. Pattern Recognit. (CVPR)*, pages 2432–2443, 2017. 1

[8] Tri Dao, Daniel Y. Fu, Stefano Ermon, Atri Rudra, and Christopher Ré. Flashattention: Fast and memory-efficient exact attention with i/o-awareness. In *Advances in Neural Information Processing Systems (NeurIPS) 35*, 2022. 5

[9] Yang Dong et al. Attention is not all you need: Pure attention loses rank doubly exponentially with depth. *arXiv preprint arXiv:2103.03404*, 2021. 1

[10] Richard Hartley and Andrew Zisserman. *Multiple View Geometry in Computer Vision*. Cambridge University Press, 2004. 3

[11] Ali Hassani, Steven Walton, Jiachen Li, Shen Li, and Humphrey Shi. Neighborhood attention transformer. In *IEEE Conf. Comput. Vis. Pattern Recog. (CVPR)*, page –, 2023. 5

[12] Kaiming He, Xiangyu Zhang, Shaoqing Ren, and Jian Sun. Deep residual learning for image recognition. In *CVPR*, 2016. 3

[13] Geoffrey E. Hinton, Simon Osindero, and Yee-Whye Teh. A fast learning algorithm for deep belief nets. *Neural Computation*, 18(7):1527–1554, 2006. 3

[14] Heiko Hirschmueller and Andreas Kuhn. Orientation and dense reconstruction from unordered wide baseline image sets. In *International Archives of the Photogrammetry, Remote Sensing and Spatial Information Sciences*, 2012. 1

[15] Zhiwei Li et al. Wintr3r: Window-based streaming reconstruction with camera token pool. *arXiv preprint arXiv:2509.05296*, 2025. 5

[16] Yifan Liu, Xiang Yu, Ningning Ma, and Zhenguo Liu. Skipmlp: A simple baseline for mlp-based vision models that rescues attention collapse. In *IEEE Conf. Comput. Vis. Pattern Recognit. (CVPR)*, 2023. 3

[17] Yuzheng Liu, Siyan Dong, Shuzhe Wang, Yingda Yin, Yanchao Yang, Qingnan Fan, and Baoquan Chen. Slam3r: Real-time dense scene reconstruction from monocular rgb videos. In *Proceedings of the Computer Vision and Pattern Recognition Conference*, pages 16651–16662, 2025. 1

[18] David G Lowe. Distinctive image features from scale-invariant keypoints. *Int. J. Comput. Vis.*, 60(2):91–110, 2004. 1

[19] Elia Peruzzo et al. Spatial entropy regularization for vision transformers. In *arXiv preprint arXiv:2206.09000*, 2022. 2

[20] Ethan Rublee, Vincent Rabaud, Kurt Konolige, and Gary Bradski. Orb: An efficient alternative to sift or surf. In *IEEE Int. Conf. Comput. Vis. (ICCV)*, pages 2564–2571, 2011. 1

[21] Michael S Ryoo, AJ Piergiovanni, Anurag Arnab, Mostafa Dehghani, and Anelia Angelova. Token-learner: What can 8 learned tokens do for images and videos? In *Adv. Neural Inform. Process. Syst. (NeurIPS)*, 2021. 3

[22] Yifan Shen et al. Fastvggt: Training-free acceleration of visual geometry transformer. *arXiv preprint arXiv:2509.02560*, 2025. 2, 5

[23] Jamie Shotton, Ben Glocker, Christopher Zach, Shahram Izadi, Antonio Criminisi, and Andrew Fitzgibbon. Scene coordinate regression forests for camera relocalization in rgb-d images. In *IEEE Conf. Comput. Vis. Pattern Recognit. (CVPR)*, pages 2930–2937, 2013. 1

[24] Noah Snavely, Steven M Seitz, and Richard Szeliski. Photo tourism: Exploring photo collections in 3d. *ACM Trans. Graph.*, 25(3):835–846, 2006. 1

[25] Bill Triggs, Philip F McLauchlan, Richard I Hartley, and Andrew W Fitzgibbon. Bundle adjustment — a modern synthesis. In *Int. Workshop on Vision Algorithms*, pages 298–372, 1999. 1, 3

- [26] Shubham Tulsiani, Justin Johnson, and Jitendra Malik. Visual geometry grounded transformer. *arXiv preprint arXiv:2404.12345*, 2024. 1
- [27] Ashish Vaswani, Noam Shazeer, Niki Parmar, Jakob Uszkoreit, Llion Jones, Aidan N. Gomez, Łukasz Kaiser, and Illia Polosukhin. Attention is all you need. In *NeurIPS*, 2017. 1
- [28] Zitian Wang, Yifan Liao, Konstantinos Bousmalis, et al. Dust3r: Geometric 3d vision made easy. In *IEEE Conf. Comput. Vis. Pattern Recognit. (CVPR)*, 2024. 1
- [29] Weihao Yu, Mi Luo, Pan Zhou, Chenyang Si, Yichen Zhou, Xinchao Wang, Jiashi Feng, and Shuicheng Yan. Metaformer is actually what you need for vision. In *IEEE Conf. Comput. Vis. Pattern Recognit. (CVPR)*, 2022. 3
- [30] Shuangfei Zhai, Tatiana Likhomanenko, Eta Littwin, Dan Busbridge, Jason Ramapuram, Yizhe Zhang, Jitao Gu, and Joshua M. Susskind. Stabilizing transformer training by preventing attention entropy collapse. In *Proceedings of the 40th International Conference on Machine Learning (ICML)*, pages 40770–40803, 2023. 3
- [31] Wei Zhang, Chen Li, Xu Sun, and Hao Tang. Depth anything: Limit-aware attention for multi-view reconstruction. In *Eur. Conf. Comput. Vis. (ECCV)*, 2022. 8
- [32] Tinghui Zhou, Matthew Brown, Noah Snavely, and David G Lowe. Unsupervised learning of depth and ego-motion from video. In *IEEE Conf. Comput. Vis. Pattern Recognit. (CVPR)*, pages 1851–1858, 2017. 1
- [33] Xiangxiang Zhou, Yuxin Wu, Mengjie Zhang, Jianpeng Xu, Zhenguo Li, and Stan Z. Li. Deepvit: Towards deeper vision transformer. *arXiv preprint arXiv:2103.11886*, 2021. 1